

Production of ϕ Mesons in Au + Au Collisions at 11.7A GeV/c

B.B. Back,¹ R.R. Betts,^{1,2} J. Chang,³ W.C. Chang,^{3,*} C.Y. Chi,⁴ Y.Y. Chu,⁵ J.B. Cumming,⁵ J.C. Dunlop,^{6,†} W. Eldredge,³ S.Y. Fung,³ R. Ganz,^{2,†} E. Garcia,⁷ A. Gillitzer,^{1,‡} G. Heintzelman,^{6,†} W.F. Henning,^{1,§} D.J. Hofman,^{1,¶} B. Holzman,^{2,†} J.H. Kang,⁸ E.J. Kim,⁸ S.Y. Kim,⁸ Y. Kwon,⁸ D. McLeod,² A.C. Mignerey,⁷ M. Moulson,^{4,**} V. Nanal,^{1,††} C.A. Ogilvie,^{6,‡‡} R. Pak,^{9,†} A. Ruangma,⁷ D.E. Russ,^{7,§§} R.K. Seto,³ P.J. Stankas,⁷ G.S.F. Stephans,⁶ H.Q. Wang,^{3,¶¶} F.L.H. Wolfs,⁹ A.H. Wuosmaa,¹ H. Xiang,³ G.H. Xu,³ H.B. Yao,⁶ and C.M. Zou^{3,***}

(E917 Collaboration)

¹Argonne National Laboratory, Argonne, IL 60439, USA

²University of Illinois at Chicago, Chicago, IL 60607, USA

³University of California, Riverside, CA 92521, USA

⁴Columbia University, Nevis Laboratories, Irvington, NY 10533, USA

⁵Brookhaven National Laboratory, Upton, NY 11973, USA

⁶Massachusetts Institute of Technology, Cambridge, MA 02139, USA

⁷University of Maryland, College Park, MD 20742, USA

⁸Yonsei University, Seoul 120-749, South Korea

⁹University of Rochester, Rochester, NY 14627, USA

We report on a measurement of ϕ -meson production in Au + Au collisions at a beam momentum of 11.7A GeV/c by Experiment 917 at the AGS. The measurement covers the midrapidity region $1.2 < y < 1.6$. Transverse-mass spectra and rapidity distributions are presented as functions of centrality characterized by the number of participant projectile nucleons. The yield of ϕ 's per participant projectile nucleon increases strongly in central collisions in a manner similar to that observed for kaons.

PACS numbers: 25.75.-q, 25.75.Dw, 13.85.Ni

I. INTRODUCTION

The production of ϕ mesons in relativistic heavy-ion collisions has been an important subject of study at the AGS, the SPS, and RHIC. The production of the ϕ meson, the lightest bound state of strange quarks ($s\bar{s}$), is suppressed in ordinary hadronic interactions because of the Okubo-Zweig-Iizuka (OZI) rule [1]. It has been proposed that in a quark-gluon plasma (QGP) scenario, strange quarks could be rapidly and abundantly

produced via gluon interactions [2]. Thus, ϕ mesons could be created in a non-conventional way via strange quark coalescence, bypassing the OZI rule. A strong enhancement in ϕ -meson production would serve as one of the strangeness-enhancement signatures for QGP formation [3].

The production of ϕ mesons has been measured in Si + Au collisions at 14.6A GeV/c by E859 at the AGS within a rapidity interval of $1.2 < y < 2.0$ [4]. The ratio of the total ϕ yield to the K^- yield has been found to be 10% for the uppermost 7% of the charged-particle multiplicity distribution. NA49 at the SPS has measured ϕ -meson production in $p + p$, $p + \text{Pb}$, and $\text{Pb} + \text{Pb}$ collisions at a beam energy (E_{beam}) of 158A GeV within a rapidity range of $3.0 < y < 3.8$. An enhancement in the ratio of ϕ to pion total yields by a factor of 3.0 ± 0.7 has been observed in central $\text{Pb} + \text{Pb}$ collisions relative to in $p + p$ interactions [5]. Also at the SPS, NA50 has measured the ratio $\phi/(\rho + \omega)$ as a function of centrality in $\text{Pb} + \text{Pb}$ collisions by fitting the invariant-mass spectrum of muon pairs with $0 < y - y_{NN} < 1$ and $1.5 < m_t \lesssim 3$ GeV/c² [6]. Both this ratio and the absolute yield of ϕ 's per participant nucleon have been found to increase significantly with the number of participant nucleons. The STAR experiment has reported on a measurement of the ϕ yield at midrapidity in Au + Au collisions at center-of-mass energy $\sqrt{s_{NN}} = 130$ GeV. An increase in the ϕ/h^- ratio with $\sqrt{s_{NN}}$ has been observed [7].

Enhancements in the yields of particles with open strangeness have also been observed. At the AGS, K^+/π^+ ratios have been seen to increase to $\sim 20\%$ in

*Present address: Institute of Physics, Academia Sinica, Taipei 11529, Taiwan.

†Present address: Brookhaven National Laboratory, Upton, NY 11973, USA.

‡Present address: Forschungszentrum Jülich, Jülich, D-52425, Germany.

§Present address: Gesellschaft für Schwerionenforschung, D-64291 Darmstadt, Germany.

¶Present address: University of Illinois at Chicago, Chicago, IL 60607.

**Present address: Laboratori Nazionali di Frascati dell'INFN, 00044 Frascati RM, Italy.

††Present address: Tata Institute of Fundamental Research, Colaba, Mumbai 400005, India.

‡‡Present address: Iowa State University, Ames, IA 50011.

§§Present address: National Institute of Health, Gaithersburg, MD 20892.

¶¶Present address: CW Associates, 7676 Woodbine, Markham L3R 2N2, Ontario.

***Present address: H.-M. Zou, Rabobank Nederland, 245 Park Ave, New York, NY 10167.

central Si + Au and Au + Au collisions, from 4–8% in $p + p$ collisions [8, 9, 10], and the $\bar{\Lambda}/\bar{p}$ ratio has been found to increase strongly with centrality in Au + Au collisions [11, 12]. At the SPS, the WA97 collaboration has observed enhanced production of K 's, Λ 's, Ξ 's, and Ω 's in heavy-ion collisions relative to in $p + p$ or $p + A$ collisions [13]. Measurements from the PHENIX experiment at center-of-mass energy $\sqrt{s_{NN}} = 130$ GeV have shown the kaon yield to be more strongly dependent on centrality than the pion yield at midrapidity [14].

The reason for the strangeness enhancement in heavy-ion collisions is not completely understood. The rescattering of hadrons and the conversion of the excitation energy of secondary resonances into strange particles might give rise to strangeness enhancement in a purely hadronic picture [15, 16, 17]. Strangeness enhancement can also be interpreted as a reduction in canonical strangeness suppression from $p + p$ to $A + A$ reactions in the context of thermal models [18]. Strangeness enhancement as a function of the number of “grey” protons (a centrality index) has also been seen in $p + A$ collisions, in which a QGP phase is unlikely to contribute [19].

Under the conventional hadronic interactions, there are mainly three scenarios proposed for the production of ϕ mesons in nuclear collisions:

- Parton fusion of strange sea quarks [20] or knock-out of $s\bar{s}$ pairs [21] from the primary collisions of projectile and target nucleons.
- Secondary baryon-baryon interactions $BB \rightarrow \phi NN$, meson-baryon interactions $(\pi, \rho)B \rightarrow \phi B$ [22] and meson-meson interactions $\pi\rho \rightarrow \phi$ [23], where $B = N, \Delta, N^*$.
- Secondary kaon-hyperon interactions $KY \rightarrow \phi N$ and kaon-antikaon scattering $K\bar{K} \rightarrow \phi\rho$ in the event of the restoration of chiral symmetry in the hot and dense nuclear fireball [24].

With inclusion of secondary meson-baryon and meson-meson interactions, RQMD (Relativistic Quantum Molecular Dynamics) [23] is able to qualitatively describe the increase of kaon yields with centrality measured by E866 [25], though quantitative differences do exist [26].

The different scenarios described above imply different relations between the scaling of ϕ production and that of other hadrons, such as kaons and pions, with collision centrality and energy. Hence, a systematic measurement of ϕ production in different collisional systems may help to quantify the increase in the overall strangeness production, and, in combination with other measurements of strange and non-strange hadron production, to differentiate between possible mechanisms contributing to the strangeness enhancement [27].

In this paper we report on a measurement of the ϕ yield around midrapidity in Au + Au collisions at the Alternating Gradient Synchrotron (AGS) at Brookhaven National Laboratory (BNL), and compare it to the yields of pions and kaons.

II. EXPERIMENTAL DETAILS

Experiment 917 took data on Au+Au reactions at projectile momenta of 6.8, 8.9 and 11.7A GeV/ c (corresponding to center-of-mass energies $\sqrt{s_{NN}} = 3.83, 4.31, \text{ and } 4.87$ GeV, respectively) in the fall of 1996. The identified particles include particles containing strange quarks, such as $K^+, K^-, \phi, \Lambda, \text{ and } \bar{\Lambda}$, and non-strange particles such as $\pi, p, \text{ and } \bar{p}$ [10, 12, 28, 29, 30]. The experimental apparatus consisted of a movable magnetic spectrometer for tracking and particle identification, and beamline detector arrays for global event characterization. When the data reported in this work were collected, the beam momentum was 11.7A GeV/ c , an Au target with areal density 1961 mg/cm² (corresponding to approximately 4% of an interaction length for an Au projectile) was used, and the spectrometer angle was set to either 14° or 19° from the beam axis. The momentum resolution of the spectrometer, $\delta p/p$, was about 1% for particles with momentum greater than 1 GeV/ c and increased at lower momentum, up to 2% at $p = 0.6$ GeV/ c , due to the effect of multiple scattering. The kaon momenta in reconstructed ϕ events lay mostly in the range of $1.0 < p < 2.0$ GeV/ c . Event centrality was characterized by the energy of the beam spectators after the interaction as measured in the zero-degree calorimeter (ZCAL), positioned downstream of the target on the beam axis. More details on the detector systems are given in Refs. [30, 31, 32].

The data presented here were collected using a two-level online trigger: a minimum-bias spectrometer-activity trigger (LVL1) followed by a particle-identification trigger (LVL2) which required two charged kaons of either sign or one \bar{p} in the spectrometer acceptance. The hardware LVL2 trigger looped over the combinations of drift chamber and TOF hits, and formed combinations consistent with tracks corresponding to particles of given momentum, charge, and particle type using a look-up table [33]. The LVL2 trigger increased the live time of the data-acquisition system by essentially the ratio of the rate of vetoable LVL1 triggers to the rate of vetoable LVL1 triggers that were not vetoed. This ratio was known as the LVL2 rejection factor, and could be estimated online. In Au + Au collisions with a magnetic field of 4 KG and the spectrometer at 14° and 19°, typical rejection factors for a $2K/\bar{p}$ trigger were 4.8 and 8.5, respectively. By examining data that was taken with the LVL1 trigger and recording the decision of the LVL2 trigger, the inefficiency of the latter was monitored and found to be less than 1% for events fully inside the acceptance. Most of the LVL2-triggered data was background since the trigger was optimized to reject only events that were clearly not of the correct type in order to keep its efficiency near 100%.

A time-of-flight (TOF) system with a typical resolution of 130 ps served to identify pions and kaons up to a momentum of 1.75 GeV/ c with 3 standard deviations of TOF resolution. Above this momentum, the 3σ contours in the (p, TOF) plane began to overlap. Within this re-

TABLE I: Centrality bins used in the analysis. The cuts on zero-degree energy, E_{ZCAL} , that define each bin are listed (in GeV), together with the corresponding fraction of the total cross section for Au + Au collisions (in percent), the mean number of projectile participants for the bin, $\langle N_{pp} \rangle$, and the estimated value of the mean number of binary collisions, $\langle N_{coll} \rangle$, by Glauber model and the mean number of projectile participants estimated from E_{ZCAL} , $\langle N_{pp}^{ZCAL} \rangle$. The total beam kinetic energy in the collisions is about 2123 GeV.

bin	E_{ZCAL}	% σ_{tot}	$\langle N_{pp} \rangle$	$\langle N_{coll} \rangle$	$\langle N_{pp}^{ZCAL} \rangle$
1	0-280	0-5	170 ± 10	770 ± 72	179 ± 1.0
2	280-560	5-12	138 ± 12	585 ± 74	157 ± 1.5
3	560-960	12-23	101 ± 14	393 ± 74	126 ± 2.0
4	960-1440	23-39	62 ± 14	207 ± 60	84 ± 2.6
5	>1440	39-77	20 ± 12	50 ± 38	34 ± 3.1

gion, particles were identified as kaons only if their TOF was inside the kaon region and outside of the pion region, since 10–30% of the tracks in the overlap region were from pions. A specific correction for the kaon-identification inefficiency from the exclusion of the pion bands in this region of high momenta was implemented in the analysis (see Sec. III B). Additionally, kaons with momenta less than 0.5 GeV/c were rejected, in order to avoid the need for large acceptance corrections.

The index of event centrality was obtained from the distribution of the energy deposited in the zero-degree calorimeter, E_{ZCAL} , obtained using a minimum-bias interaction trigger based on the measurement with a Čerenkov counter of the projectile charge after passage through the target. Empty-target runs were periodically taken in order to subtract the background from the ZCAL energy distribution. Assuming a monotonic relation between the energy deposition in the calorimeter and the event centrality such that the most central events correspond to the smallest energy deposition, we divided the data into five centrality bins. The centrality bins are expressed as a fraction of the total cross section for Au + Au collisions, 6.8 b as evaluated from the parameterizations of Ref. [34]. The cross section for Au + Au collisions as measured with the minimum-bias interaction trigger is approximately 5.2 b, or 77% of the total cross section.

We have attempted to estimate $\langle N_{pp} \rangle$, the mean number of projectile participants, and $\langle N_{coll} \rangle$, the mean number of binary collisions, according to the Glauber model [35], using impact parameter cuts corresponding to the centrality range for each bin as listed in Table I, and an assumed $p + p$ inelastic cross section of 30 mb. In Experiments 802, 856 and 866 [9], the number of projectile participants has been conventionally estimated from the relation $N_{pp}^{ZCAL} = A_{proj}(1 - E_{ZCAL}/E_{beam})$, where A_{proj} is the atomic mass of the projectile, and E_{beam} is the total kinetic energy of the nuclei in the beam before interaction, which was 2123 GeV in the present case. For the purpose of comparison, we have also calculated N_{pp}^{ZCAL} and its uncertainty with a nominal ZCAL energy

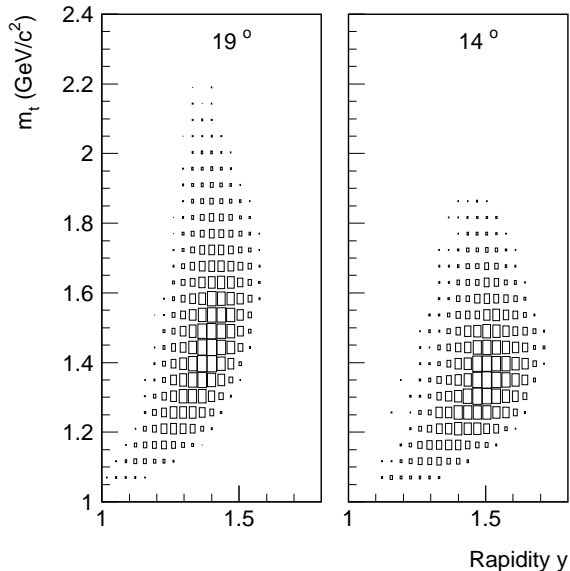


FIG. 1: The experimental acceptance for K^+K^- pairs in the space of transverse mass (m_t) vs. rapidity (y) for the 19° and 14° spectrometer angle settings.

resolution (σ_E/E) of 3.6% [36]. All relevant parameters for each centrality bin are listed in Table I. To facilitate comparison with other experiments we will use $\langle N_{pp} \rangle$ as calculated using the Glauber model for the rest of this paper.

III. EXPERIMENTAL RESULTS

A total of 250 million LVL2-triggered events were analyzed. When the two spectrometer angle settings were combined, the overall acceptance for K^+K^- pairs covered the region of rapidity $1.2 < y < 1.6$ and transverse mass $1.0 \text{ GeV}/c^2 < m_t \equiv [m_\phi^2 + (p_t/c)^2]^{1/2} < 2.2 \text{ GeV}/c^2$, as shown in Fig. 1.

The ϕ mesons were reconstructed by forming the invariant-mass (m_{inv}) distribution of identified K^+K^- pairs and subtracting the combinatorial background, which was obtained by the event-mixing method [37]. Two kinds of distributions were formed: “same-event” distributions, in which the K^+ ’s and K^- ’s were selected from the same event, and “mixed-event” distributions, in which the individual particles were chosen from different events in the same centrality class to represent the uncorrelated background.

A. Invariant-mass distribution for K^+K^- pairs

First, we examined the minimum-bias invariant-mass distribution of kaon pairs by fitting the data to a relativis-

tic Breit-Wigner distribution (RBW) convoluted with a Gaussian representing the experimental mass resolution [4, 38]. The shape of the background (BG) was obtained from the mixed-event distribution while the normalization was left as a free parameter in the fit. The parameterization is as follows:

$$\frac{dN_{K^+K^-}^{\text{same}}}{dm} = a \int_{m_1}^{m_2} \text{RBW}(m') \frac{\exp\left[-\frac{1}{2}\left(\frac{m-m'}{\sigma_m}\right)^2\right]}{\sqrt{2\pi\sigma_m^2}} dm' + b \frac{dN_{K^+K^-}^{\text{mixed}}}{dm}, \quad (1)$$

where

$$\text{RBW}(m) = \frac{mm_0\Gamma(m)}{(m^2 - m_0^2)^2 + (m_0\Gamma(m))^2}, \quad (2)$$

$$\Gamma(m) = 2\Gamma_0 \frac{(q/q_0)^3}{(q/q_0)^2 + 1}, \quad (3)$$

$$q_0 = \sqrt{m_0^2/4 - m_K^2}, \quad (4)$$

$$q = \sqrt{m^2/4 - m_K^2}, \quad (5)$$

and where the limits of integration were $m_1 = 0.989 \text{ GeV}/c^2$ and $m_2 = 1.252 \text{ GeV}/c^2$. There were five free parameters in all: the relative normalizations a and b , the peak mass and width parameters m_0 and Γ_0 , and the experimental mass resolution σ_m .

For the minimum-bias data, the same-event invariant-mass distribution of K^+K^- pairs and the background-subtracted signal distribution corresponding to the first term in Eq. (1) are shown together with the fits in Fig. 2. The values $m_0 = 1018.99 \pm 0.36 \text{ MeV}/c^2$, $\Gamma_0 = 6.14 \pm 2.59 \text{ MeV}/c^2$, and $\sigma_m = 2.43 \pm 1.11 \text{ MeV}/c^2$ were obtained with $\chi^2/\text{dof} = 145/167 = 0.87$. The fit results for the peak position (m_0) and width (Γ_0) of the ϕ signal are in agreement with the world-average values. The large uncertainty on Γ_0 arises mostly because of a high degree of correlation in the fit between the values for the parameters Γ_0 and b (correlation coefficient = 0.71). The value obtained for the experimental mass resolution (σ_m) is also consistent with our estimated value of $2.0 \text{ MeV}/c^2$, from Monte Carlo studies and from the width of the peak from Λ decay in the $p\pi^-$ invariant-mass distribution [32] (the known contribution from the multiple scattering of the kaons in the target in the case of the present measurement was accounted for by additional smearing). It is noted that the result of the fit lies systematically below the data in the invariant-mass region 10–20 MeV/c^2 below the ϕ peak. We do not have a clear understanding of this effect.

B. Signal counting and extraction of differential yields

Monte Carlo studies confirm that the experimental invariant-mass resolution (σ_m) remains constant

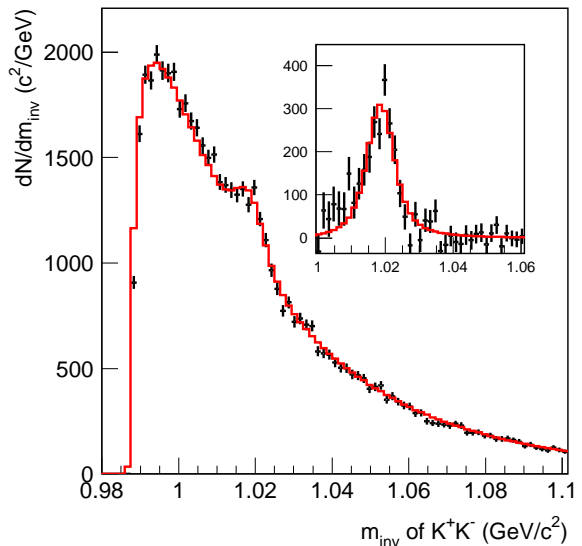


FIG. 2: (Color Online) The invariant-mass (m_{inv}) distribution of K^+K^- pairs for minimum-bias events, superimposed with a fit consisting of a relativistic Breit-Wigner distribution plus the background distribution from a mixed-event technique, as described in the text. In the inset, the ϕ signal together with fit results from the first term in Eq. (1) is shown.

($\sim 2 \text{ MeV}/c^2$) across the kinematic region of acceptance [32]. Given the stable mass resolution and the limited statistics for the division of data into bins in centrality and phase space, the transverse-mass spectra were obtained by counting events in a defined signal window and estimating the number of background events within this window, rather than by integration of the result of the fit with Eq. (1). The details were as follows. The data were divided into subsets for each of the two spectrometer settings and five centrality classes. Same-event and mixed-event pairs for each subset were binned in rapidity and transverse mass ($\Delta y = 0.2$ and $\Delta m_t = 0.2 \text{ GeV}/c^2$), and invariant-mass distributions were obtained for each bin. No corrections were applied to the invariant-mass distributions at this stage—signal extraction was performed on the spectra of raw counts. In each bin, the total number of signal and background counts ($S + B$) was taken to be the sum of the counts within a signal window defined as $1.0040 < m_{inv} < 1.0355 \text{ GeV}/c^2$. In units of the natural ϕ width, this interval corresponds to approximately $\pm 3.7\Gamma_0$ about the expected peak position. We then estimated the number of background counts (B) inside the signal window as the number of counts in the normalized distribution of mixed-event pairs in this same interval. For this purpose, the mixed-event distributions were normalized to have the same area outside of the signal window as the same-event distributions. The final number of signal counts (S) was obtained by subtract-

ing the background estimated in this way from the total number of events in the signal window. Using this procedure, we were able to obtain estimates of S for a total of 88 distributions corresponding to different bins in phase space and centrality for each of the two angle settings.

We use the χ^2 statistic obtained from the Poisson log-likelihood treatment described in Ref. [39] as an index of the degree of consistency between the same- and mixed-event invariant-mass distributions in the mass region used for normalization. We typically found $\chi^2/\text{dof} \approx 0.8$ (for most fits, the number of degrees of freedom—one minus the number of populated bins outside of the signal window in the mixed-event distributions—was 149). In the worst case, we found $\chi^2/\text{dof} = 177/149$.

The statistical error on S was calculated as $\sigma_S^2 = (S + B) + \sigma_B^2$. Here, $(S + B)$ is the contribution from Poisson fluctuations in the number of total counts in the signal window, and σ_B was taken to be $B/\sqrt{B_{\text{out}}}$, with B_{out} the number of counts in the spectra *outside* the signal window (where same- and mixed-event spectra are normalized to the same integral). As an index of the statistics of the measurement, the values obtained for S range from a few counts for bins in phase space near the limits of the spectrometer acceptance, to approximately 100 counts for bins well within the acceptance. Typical values of the signal-to-total ratio, $S/(S + B)$, were 0.05–0.30; 74 of the 88 measurements had values of $S/(S + B)$ within this interval. The median statistical error for the 88 measurements of S was 72%; 57 of the 88 measurements had statistical errors of less than 100%.

Systematic errors on S may result if the signal window does not completely include the signal peak. In this case, not only are the tails of the signal peak excluded from the signal count—the equal-area normalization technique will also cause the baseline to be overestimated. Systematic errors on S may also arise if the mixed-event distributions do not accurately represent the background in the same-event distributions. Of particular concern is the excess of counts in the mass interval 1.000–1.010 GeV/c^2 noted in Sec. III A and visible in Fig. 2. In the same-event spectra for the individual centrality and phase-space bins, this excess is present to varying degrees. Since we are uncertain of the origin of this excess, its effects must be included in our estimates of the systematic error for the signal count in each bin.

We assign the systematic error on S for each bin by varying the width of the signal window from $\pm 2\Gamma_0$ to $\pm 5\Gamma_0$. For window sizes smaller than $\pm 2\Gamma_0$, the signal count drops precipitously. For window sizes larger than $\pm 5\Gamma_0$, there is very little constraint on the normalization from the low-mass portion of the distribution. In Fig. 3 we show the dependence of S on the width of the signal window for minimum-bias distributions in six bins of y and m_t . For each bin, values of S are plotted for nine different choices for the signal window, each symmetric about the expected peak position with half-width in units of Γ_0 given by the abscissa value. The central point in each plot, corresponding to a window width of

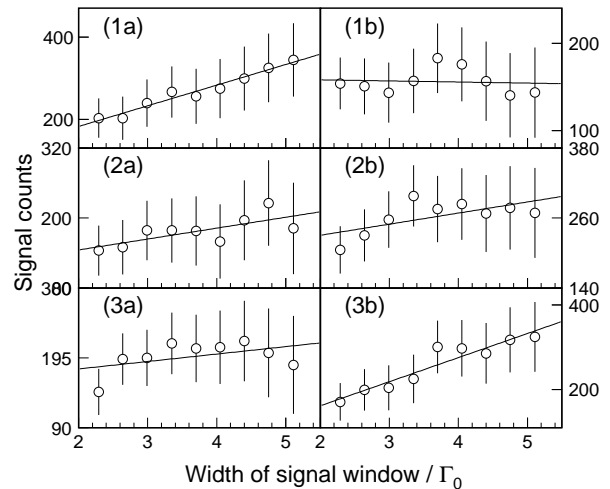


FIG. 3: Dependence of S on width of signal window for six bins in y and m_t : 1a) $1.2 < y < 1.4$, $1.5 < m_t < 1.7 \text{ GeV}/c^2$, 2a) $1.2 < y < 1.4$, $1.7 < m_t < 1.9 \text{ GeV}/c^2$, 3a) $1.4 < y < 1.6$, $1.7 < m_t < 1.9 \text{ GeV}/c^2$, 1b) $1.2 < y < 1.4$, $1.3 < m_t < 1.5 \text{ GeV}/c^2$, 2b) $1.4 < y < 1.6$, $1.3 < m_t < 1.5 \text{ GeV}/c^2$, and 3b) $1.4 < y < 1.6$, $1.5 < m_t < 1.7 \text{ GeV}/c^2$. For panels 1a, 2a, and 3a, the spectrometer was at 19° ; for panels 1b, 2b, and 3b, the spectrometer was at 14° . Minimum-bias data (0–77% central) are shown in each case. The abscissa is the half-width of the signal window expressed in units of the ϕ width, $\Gamma_0 = 4.26 \text{ MeV}/c^2$. The errors plotted are statistical only. The lines represent the results of linear, least-squares fits to the points, using uniform weights, and are used to obtain the estimate of the systematic error on S for each bin.

about $\pm 3.7\Gamma_0$, provides the value of S used to obtain the results presented in this work. Some of the point-to-point fluctuation is statistical in nature and is presumably accounted for in the statistical errors associated with each value of S . In most cases, however, there is a suggestion of an underlying systematic trend. To quantify this trend, we perform a linear, least-squares fit with uniform weights to the nine points for each bin. The results are shown as the straight lines in the figure. For each bin, we quote as the systematic error on S the RMS variation of this line over the interval spanned by the first and last points, which is equal to the maximum vertical extent divided by $\sqrt{12}$. When applied to each centrality and phase-space bin used for the analysis, this procedure leads to systematic errors for S that vary significantly from bin to bin. For the 88 individual measurements of S , the median systematic error is 16%; 62 of the 88 measurements have systematic errors of less than 30%. In all cases, the statistical errors on S are larger than the systematic errors.

The differential yields for each bin in phase space and centrality were then calculated from S as

$$\frac{1}{m_t} \cdot \frac{d^2N}{dy dm_t} = \frac{1}{\Delta y \Delta m_t} \cdot \frac{S}{f_{\text{ZCAL}} N_{\text{INT}}} \cdot \frac{\langle a \rangle \langle w \rangle}{\text{BR} \langle m_t \rangle} \quad (6)$$

where f_{ZCAL} is the fraction of minimum-bias interaction

triggers satisfying the centrality selection, N_{INT} is the background-subtracted number of minimum-bias interaction triggers collected with the data for normalization purposes, $\langle a \rangle$ is the geometrical acceptance correction, $\langle w \rangle$ is the overall correction factor for other experimental effects, $\langle m_t \rangle$ is the mean value of m_t for all pairs in the bin, and $\text{BR}(\phi \rightarrow K^+K^-) = 49.2\%$.

Apart from the systematic error on S , the principal source of systematic uncertainty in the yields is from the uncertainty on f_{ZCAL} . Due to radiation damage to the plastic-scintillator materials of the ZCAL, its signal decreased with time. A run-dependent calibration was therefore used, in which the energy of the fragmented-beam peak was recentered at the nominal beam kinetic energy (with corrections for energy loss in the target). These calibrations were performed periodically throughout the running period. The centrality bins were then defined via fixed cuts on the calibrated ZCAL energy. However, f_{ZCAL} exhibited residual variation as a function of running time. The resulting contributions to the systematic errors on the yield measurements are estimated to range from about 5% in the most central bin to 10% for the most peripheral bin.

The geometrical acceptance, $\langle a \rangle$, and many of the contributions to the weight factor $\langle w \rangle$, were calculated using a GEANT-based Monte Carlo simulation implementing a realistic detector configuration [32]. The value of $\langle a \rangle$ used in Eq. (6) is the average value for $\phi \rightarrow K^+K^-$ events in the phase-space bin of interest. The weight factor $\langle w \rangle$ was calculated as follows for each centrality and phase-space bin. Corrections for kaon decays in flight, the single-particle tracking inefficiency, hadronic interactions, multiple scattering in the spectrometer, momentum cuts, and the kaon-identification inefficiency were evaluated using the Monte Carlo, separately for each track in each pair. An additional correction for the single-track tracking efficiency in the presence of background hits on the drift chambers was evaluated by inserting found tracks into random events. This occupancy correction was then parameterized by the hit multiplicity in the chambers and applied for each track; the resulting correction was typically 20–40%. The individual correction weights for each track and from each of the above sources were then multiplied, together with an additional correction for a two-track opening-angle cut (evaluated for each pair), to obtain the overall pair weight, w . The value of $\langle w \rangle$ in Eq. (6) is the average value of w for all pairs in the same-event distribution of interest. The systematic errors associated with $\langle a \rangle$ and $\langle w \rangle$ are estimated to be no larger than 5%, arise mainly from the statistics of the samples used to obtain the weight factors, and do not significantly affect the results.

The final systematic errors on the individual yield measurements are calculated as the quadrature sum of the fractional systematic errors on S (for each measurement), on f_{ZCAL} (for each centrality bin), and on $\langle a \rangle \langle w \rangle$ (constant). In general, the dominant contribution is from the systematic uncertainty on S . For the 88 individual differ-

ential yield measurements, the median overall systematic error is 20%; 60 of the 88 measurements have systematic errors of less than 30%, and 75 of the 88 have systematic errors of less than 50%. In all cases, the statistical errors are larger than the overall systematic errors; for 73 of the 88 measurements, the statistical errors are more than twice as large as the overall systematic errors.

Experimental results from both the 14° and 19° settings of the spectrometer were in all cases consistent within statistical errors, and were therefore combined for the presentation of the transverse-mass spectra, resulting in the 53 individual differential yield measurements plotted in Fig. 4.

C. Transverse-mass spectra and rapidity distributions

The transverse-mass spectra for the five centrality bins are shown in two bins of rapidity, $1.2 < y < 1.4$ and $1.4 < y < 1.6$, with an m_t bin size of $0.2 \text{ GeV}/c^2$, in Fig. 4. For the m_t bins where the acceptance from 14° and 19° data sets overlap, the individual measurements from each of the data sets agree to within statistical errors, and the weighted average of the two measurements is presented. The full error shown includes both statistical and systematic contributions; the contribution from statistics alone is indicated by the cross bars. The total errors are calculated as the quadrature sum of the statistical and systematic errors.

An exponential parameterization with two parameters, rapidity density (dN/dy), and inverse slope (T), was used to fit the transverse-mass spectra:

$$\frac{1}{2\pi c^4 m_t} \frac{d^2 N}{dm_t dy} = \frac{dN/dy}{2\pi(Tm_0 c^2 + T^2)} \times \exp\left[-\frac{(m_t - m_0)c^2}{T}\right]. \quad (7)$$

This function gave a good fit to the data with $\chi^2/\text{dof} \sim 1$ in all cases. The values obtained for the rapidity density (dN/dy) and inverse-slope parameters (T) are plotted as functions of rapidity and centrality in Fig. 5 and are listed in Tables II and III. The statistical and systematic contributions to the error were evaluated by performing the fits with and without the systematic contribution included in the errors. The systematic error due to uncertainties in the overall normalization is excluded from the systematic error estimate for T .

As a function of centrality, the rapidity density shows a strong systematic increase, while the inverse slope increases more mildly. Within the rapidity range covered by the measurement, there seems to be no strong rapidity dependence for T .

The fiducial yield is the sum of the values $dN/dy \times \Delta y$ for the two rapidity bins covering the interval $1.2 < y < 1.6$ and is plotted as a function of $\langle N_{\text{pp}} \rangle$ (calculated from

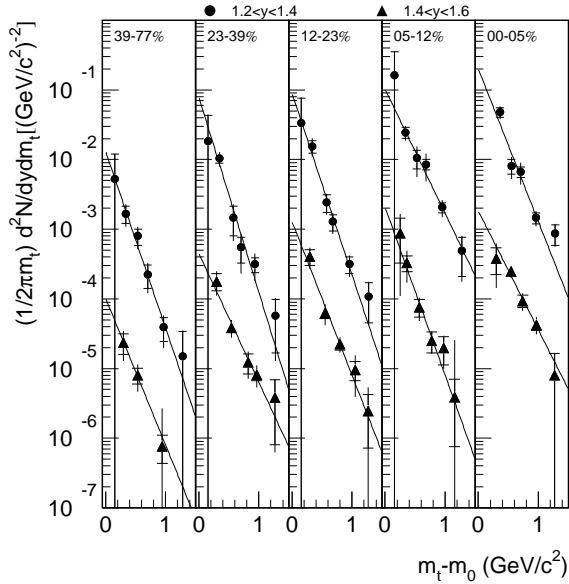


FIG. 4: The invariant yield of ϕ 's as a function of transverse mass ($m_t - m_0$) in five centrality bins labeled by $\sigma/\sigma_{\text{tot}}$. In each panel, the top set of points (circles) is for $1.2 < y < 1.4$, while the second set of points (triangles) is for $1.4 < y < 1.6$ and is divided by 100 for presentation. The total errors are calculated as the quadrature sum of the systematic and statistical errors, while the magnitudes of the latter are indicated by the cross bars. The lines are the results of the exponential fits described in the text.

a Glauber model as explained in Sec. II) in Fig. 6. When normalized to $\langle N_{\text{pp}} \rangle$, this quantity exhibits a steady increase with increasing centrality. This implies that the fiducial yield of ϕ 's increases faster than linearly with $\langle N_{\text{pp}} \rangle$. It is noted that the increase with centrality is slightly more significant (the effect is on the order of 4% in the slope of a linear fit) if the fiducial yields are plotted against $\langle N_{\text{pp}}^{\text{ZCAL}} \rangle$. Thus, we observe an enhancement in ϕ -meson production in central events. This is similar to what has been previously observed for kaon production [9]. In Pb + Pb collisions at the SPS, NA50 has also observed an increase in the yield of ϕ 's per participant nucleon ($\langle n_{\text{p}} \rangle$) as a function of $\langle n_{\text{p}} \rangle$ [6], though the NA50 data show more evidence of saturation of this quantity in the most central collisions than do our results.

IV. DISCUSSION

In this section, we compare the measured inverse slopes (T) and rapidity densities (dN/dy) for the ϕ to those of the other hadrons and explore their dependence on centrality and beam energy.

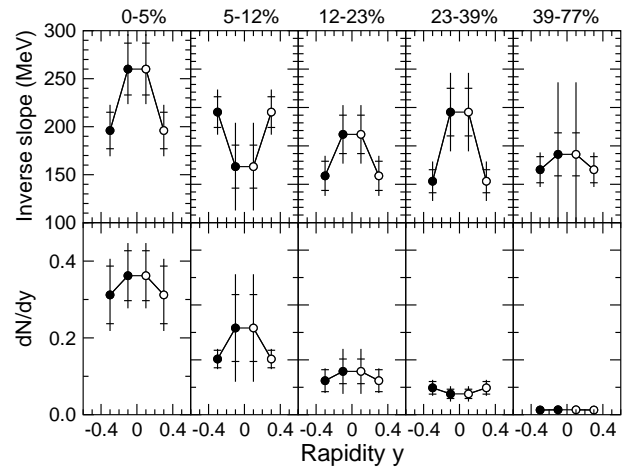


FIG. 5: The inverse-slope parameters, T , and rapidity density, dN/dy , of ϕ mesons as a function of centrality. The open symbols show the reflections of the data points about midrapidity ($y = 1.6$). The error bars have the same significance as in Fig. 4.

TABLE II: Inverse-slope parameter, T , in units of MeV/c^2 , for ϕ 's in two bins of rapidity and five bins of centrality. Errors are statistical followed by systematic.

Centrality	$1.2 < y < 1.4$	$1.4 < y < 1.6$
0-5%	$196 \pm 19 \pm 19$	$260 \pm 27 \pm 25$
5-12%	$244 \pm 20 \pm 22$	$173 \pm 28 \pm 50$
12-23%	$161 \pm 18 \pm 19$	$215 \pm 28 \pm 25$
23-39%	$154 \pm 15 \pm 21$	$244 \pm 31 \pm 40$
39-77%	$169 \pm 17 \pm 15$	$189 \pm 28 \pm 90$

A. Transverse-mass spectrum of the ϕ ; comparison to other species

In the most central bin ($\sigma/\sigma_{\text{tot}} = 0-5\%$), the inverse-slope parameter is determined to be $260 \pm 37 \text{ MeV}/c^2$ around midrapidity. As motivated by hydrodynamic models [40], the inverse-slope parameters for different particle species are expected to scale with species mass for particles that participate in the collective transverse flow. It is interesting to see whether the inverse slope for

TABLE III: Rapidity density, dN/dy , for ϕ 's in two rapidity bins, by centrality. Errors are statistical followed by systematic.

Centrality	$1.2 < y < 1.4$	$1.4 < y < 1.6$
0-5%	$0.312 \pm 0.075 \pm 0.056$	$0.362 \pm 0.065 \pm 0.054$
5-12%	$0.203 \pm 0.032 \pm 0.018$	$0.316 \pm 0.122 \pm 0.153$
12-23%	$0.124 \pm 0.040 \pm 0.020$	$0.158 \pm 0.045 \pm 0.069$
23-39%	$0.098 \pm 0.023 \pm 0.018$	$0.076 \pm 0.017 \pm 0.022$
39-77%	$0.017 \pm 0.005 \pm 0.004$	$0.018 \pm 0.005 \pm 0.005$

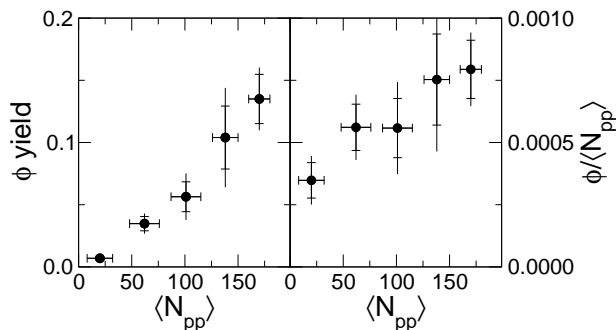


FIG. 6: The fiducial ϕ yield (left) and fiducial ϕ yield per projectile participant, $\langle N_{pp} \rangle$, as a function of $\langle N_{pp} \rangle$ (right). The accepted rapidity region is $1.2 < y < 1.6$. The error bars have the same significance as in Fig. 4.

ϕ mesons fits into the systematic trend observed for the other hadrons. However, two known effects complicate the interpretation.

The first is that the cross sections for ϕ interactions in the collision medium are expected to be small. The OZI rule inhibits elastic scattering of the ϕ on nucleons and non-strange mesons and resonances. Elastic-scattering cross-sections are dominated by Pomeron exchange and are expected to be on the order of 1 mb (see [3] and references therein). In particular, from studies of ϕ photoproduction, total cross sections for the interaction of ϕ 's with nucleons are estimated to be 8–12 mb over the range of ϕ kinetic energies from a few hundred MeV up to several GeV, and dominated by OZI-allowed absorptive processes—elastic scattering of ϕ 's on nucleons accounts for about 1 mb of this cross section [41]. It might therefore be expected that ϕ 's decouple rather early from the nuclear fireball, which is composed of nucleon resonances, pions, and non-strange meson resonances. If this were the dominant effect, the ϕ inverse slope (T) would reflect the original “temperature” when the ϕ 's are produced, without the enhancement from collective transverse flow developed in the late hadronic stages [42]. In this case, T for the ϕ 's would be lower than that observed for other hadrons of similar mass (for example, p 's).

On the other hand, when the ϕ is detected via its decay into kaons, the rescattering of the daughter kaons from ϕ 's that decay inside the nuclear fireball would generate a relative depletion in the ϕ yield at low p_t . This explanation has been proposed [43] to explain the difference in the values of T for ϕ mesons obtained by experiments NA49 and NA50, which observed the ϕ via its decay into K^+K^- and $\mu^+\mu^-$ final states, respectively. Given the short lifetime of the ϕ ($c\tau = 45$ fm/c), one might expect that this effect can give rise to a significant depletion in the m_t spectrum only at low m_t . To illustrate, we have performed a simple simulation in which ϕ 's are generated at the center of a “fireball” according to an exponential m_t distribution with $T = 250$ MeV/ c^2 , and any ϕ 's that decay within 7 fm of the origin are suppressed. For $m_t - m_0 > 0.5$ GeV/ c^2 the resulting depression of the m_t

spectrum is nearly uniform; a deficit in the spectrum of more than 10% is noted only for $m_t - m_0 \lesssim 0.25$ GeV/ c^2 , *i.e.*, only at the edge of the E917 acceptance. (A calculation performed with RQMD for Pb + Pb collisions at the SPS gives similar results [44].) Conceivably, however, in-medium effects could broaden the ϕ enough to cause a more significant fraction of ϕ 's to decay inside the fireball, leading to an increase in the apparent value of T in fits to the m_t spectra (see Ref. [45] for an example with reference to the NA49 and NA50 data).

For the comparison of the transverse-mass spectra for various particle species, we choose to use the mean transverse mass, $\langle m_t \rangle$. This is because a variety of forms are used to fit and parameterize the transverse-mass spectra in the existing measurements of π^+ [46], K^+ [9], p [30, 47], d [47], and $\bar{\Lambda}$ [12] production at midrapidity in central Au + Au collisions at the AGS, including Boltzmann, Boltzmann plus exponential, and m_t -scaled exponential forms, in addition to the simple single-exponential form used to fit the m_t spectra for ϕ 's in this work. In all but two of the reports referenced above, $\langle m_t \rangle$ is derived from the slope parameters for the chosen parameterization of the m_t spectra, and quoted in place of the slope parameters themselves. The exceptions are the K^+ and $\bar{\Lambda}$ data. In Ref. [9], the m_t spectra for kaons are fit with exponential distributions, and values of T are reported. We convert to $\langle m_t \rangle$ using the expression

$$\langle m_t \rangle_{\text{exp}} = \frac{m_0^2 c^4 + 2m_0 c^2 T + 2T^2}{m_0 c^2 + T}. \quad (8)$$

We use the same expression to obtain $\langle m_t \rangle$ from the value of T obtained from the fit to the m_t spectrum for the ϕ presented in this work. In Ref. [12], the m_t spectra for $\bar{\Lambda}$'s are fit with Boltzmann distributions,

$$\frac{1}{2\pi c^4 m_t} \frac{d^2 N}{dm_t dy} = \frac{dN/dy}{2\pi(T_B m_0^2 c^4 + 2T_B^2 m_0 c^2 + 2T_B^3)} \times m_t c^2 \exp\left[-\frac{(m_t - m_0)c^2}{T_B}\right], \quad (9)$$

and values for T_B are quoted. We convert to $\langle m_t \rangle$ using the expression

$$\langle m_t \rangle_{\text{Boltz}} = \frac{m_0^3 c^6 + 3m_0^2 c^4 T_B + 6m_0 c^2 T_B^2 + 6T_B^3}{m_0^2 c^4 + 2m_0 c^2 T_B + 2T_B^2}. \quad (10)$$

The values of $\langle m_t - m_0 \rangle$ for ϕ mesons, together with the corresponding values for π^+ 's, K^+ 's, p 's, d 's, and $\bar{\Lambda}$'s are plotted as a function of species mass in Fig. 7. We note that the centrality selection differs somewhat from species to species in the available data: top 3% for π^+ , p (E866), and d ; top 5% for p (E917), ϕ and K^+ ; and top 12% for $\bar{\Lambda}$. The rapidity coverage varies similarly: for the π^+ data it is $1.3 < y < 1.4$; for the K^+ and ϕ data it is $1.4 < y < 1.6$, for the p and d data it is $1.4 < y < 1.5$, and for the $\bar{\Lambda}$ data it is $1.0 < y < 1.4$. (For reference, $y_{NN} = 1.61$ for 11.7A GeV/c Au + Au collisions.) The dashed line in Fig. 7 shows a fit to

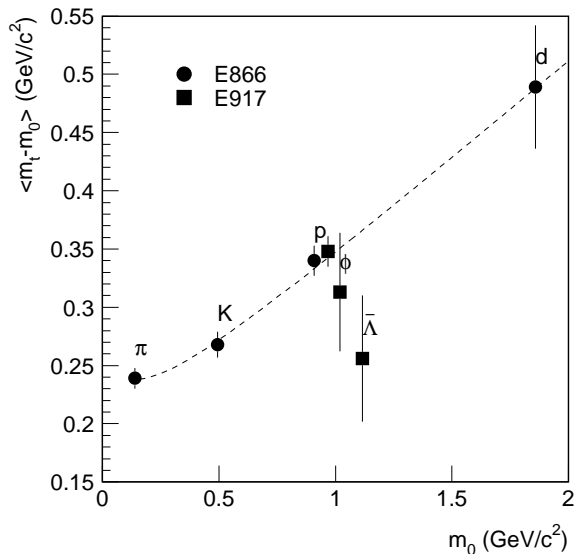


FIG. 7: The mean transverse mass ($\langle m_t - m_0 \rangle$) for various particle species as a function of the species mass at midrapidity for central Au + Au collisions at 11.7 GeV/c per nucleon as measured by E866 and E917. The dashed line is a fit assuming exponential transverse-mass spectra and a linear relationship between inverse slope (T) and particle mass (m_0), as described in the text. Values of T for particles other than the ϕ are taken from Refs. [9, 12, 30, 46, 47]. The proton data point from E866 (E917) is presented with a shift of -30 MeV/c² ($+30$ MeV/c²) in mass for clarity.

the values for $\langle m_t - m_0 \rangle$ using the form of Eq. (8) with $T = a + bm_0c^2$, so that a and b are the free parameters of the fit. Assuming that it is qualitatively valid to describe the midrapidity m_t spectra for the various species by exponential inverse-slope parameters, this fit illustrates the trend expected for a linear relationship between inverse slope (T) and particle mass (m_0), as motivated by hydrodynamic models.

The value of $\langle m_t - m_0 \rangle$ for the ϕ falls slightly below the systematic trend observed for the other particles, but less so than for $\bar{\Lambda}$'s. There may be some suggestion of an effect from early freeze-out of the ϕ and late development of at least some of the transverse flow, as described in Ref. [42]. However, the significance of this observation is limited by the precision of the measurement.

B. Centrality dependence of ϕ production; comparison to other species

As mentioned in Sec. I, processes such as $pp \rightarrow pp\phi$ are suppressed by large threshold energies and the OZI effect. Thus a naive expectation assuming ordinary hadronic interactions is that if an enhancement in ϕ production were observed in heavy-ion collisions at AGS energies, this en-

hancement would result from secondary collisions, *e.g.* via channels such as $K^+\Lambda \rightarrow \phi p$ or $K^+K^- \rightarrow \phi p$ [24]. If this were in fact the case, increasing KY and $K\bar{K}$ combinatorics would bring about an increase of the ϕ/K ratio for central collisions.

On the other hand, the proposed “re-arrangement” [20] or “shake-out” [21] of an intrinsic $s\bar{s}$ component of the nucleon wave function in the non-perturbative regime provides a mechanism for ϕ production in N + N interactions that bypasses the effects of OZI suppression. If the $s\bar{s}$ component of the nucleon wave function were negatively polarized, the fact that, at threshold, the reaction $pp \rightarrow pp\phi$ must proceed with the pp initially in the 3S_1 spin state would imply that this mechanism should be particularly important at near-threshold energies (see Ref. [48] and references therein, especially [49]). Indeed, the DISTO collaboration has observed that in $p + p$ collisions at $\sqrt{s} = 2.90$ GeV, only 83 MeV above threshold, the ϕ/K^- ratio is about unity, such that ϕ production represents an important contribution to the K^- yield at these energies [48].

Along these lines, a possible mechanism has been proposed to explain overall strangeness production in N + A collisions within the framework of the additive quark model [50]. According to this proposal, strange particles are born as strange-quark pairs from binary collisions of the projectile and target nucleons, with a probability proportional to the number of interacting constituent projectile quarks [51]. In $p + A$ collisions at 17.5 GeV/c, E910 has shown that the production of Λ 's and K_S 's increases with the estimated number of binary collisions, ν , suffered by the incident proton [19]. For $\nu \leq 3$, the increase in the yields is faster than expected from scaling of $p + p$ data by the number of total participants (*i.e.*, $N_{p+A}/N_{p+p} = \frac{1}{2}(1 + \nu)$), although bounded from above by linear scaling with ν (*i.e.*, $N_{p+A}/N_{p+p} = \nu$).

If the same mechanism were responsible for the observed increase in ϕ production with centrality in A + A collisions, we would expect to observe similar scaling behavior in our data. Specifically, we would expect approximately constant numbers of hadrons bearing strange quarks to be produced per binary collision. In the following, we therefore compare the yield of ϕ 's to the yields of pions and kaons as a function of centrality. The yields of pions and kaons were obtained by the E866 collaboration from Au + Au collisions at the same beam energy used for the present measurement [9, 46].

As seen from the left panel of Fig. 8, the ϕ/π ratio of fiducial yields shows a rise toward central collisions, which signals an enhancement in the production of ϕ mesons relative to that of non-strange π mesons in central collisions. This enhancement is also clearly suggested by Fig. 6, since pion production is known to mainly come from resonance decay and secondary rescattering and scales linearly with $\langle N_{pp} \rangle$. Due to the fact that the plotted points represent ratios of fiducial yields, some care should be taken when interpreting the exact form of the dependence. We note that this increase in the ϕ/π

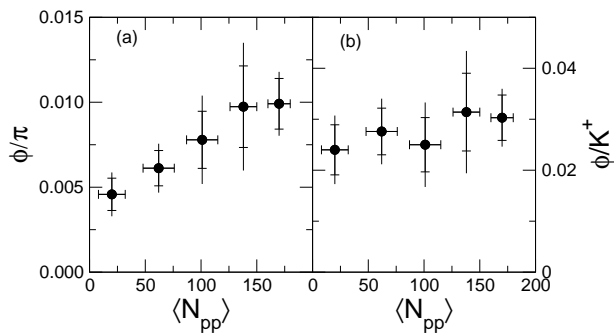


FIG. 8: The ϕ/π and ϕ/K^+ ratios as a function of $\langle N_{pp} \rangle$. For the ϕ , the fiducial yields from E917 in the rapidity interval $1.2 < y < 1.6$ are used. For π 's, the data have been taken from Ref. [46], and represent fiducial yields in the rapidity interval $1.2 < y < 1.4$. The value used for the π yield is 1.125 times the yield for π^+ and π^- [52]. For K^+ 's, the data have been taken from Ref. [9], and represent fiducial yields in the rapidity interval $1.2 < y < 1.6$.

ratio is qualitatively similar to the increase in the K/π ratio with centrality observed by E866 in Au + Au collisions at the AGS [46].

We next compare the degree of enhancement in the yields of ϕ 's and K 's, which both contain s quarks. We use the yield of K^+ to characterize the overall kaon production because the E866 data indicate that the K^-/K^+ ratio is about 0.15 and independent of centrality. In the right plot of Fig. 8, the ratio of fiducial yields ϕ/K^+ is plotted as a function of centrality, and shows no substantial variation. This implies that both ϕ and K^+ (or K^-) possess a similar degree of enhanced production toward central collisions at AGS energies. As estimated from linear fits to the ϕ/K^+ ratios as a function of $\langle N_{pp} \rangle$, an increase of up to 50% for the ratio in the most central bin cannot be definitively ruled out within a 1σ range of the fit errors. However, any centrality dependence of the ϕ/K ratios appears to be weak.

To look for scaling behavior similar to that observed in $p + \text{Au}$ collisions by E910, we examine the dependence of the ϕ yields in our data on the mean number of binary collisions, $\langle N_{coll} \rangle$. (Estimation of $\langle N_{coll} \rangle$ is discussed in Sec. II; the values of $\langle N_{coll} \rangle$ for each centrality bin are given in Table I.) The fiducial ϕ yield normalized to $\langle N_{coll} \rangle$ is plotted versus $\langle N_{coll} \rangle$ in Fig. 9. The dependence of the fiducial ϕ yield on $\langle N_{coll} \rangle$ is consistent with scaling proportional to $\langle N_{coll} \rangle$.

While the rapidity coverage of our measurement does not allow us to make a precise statement about the absolute value of the ϕ yield, it is possible to make an informed guess about the width of the ϕ rapidity distribution. Both E859 [4] and NA49 [5, 53] have observed that the Gaussian width of the ϕ rapidity distribution is very similar to those of the K^+ and K^- rapidity distributions. In central Au + Au collisions at the AGS, the Gaussian widths of the rapidity distributions for K^+ and K^- are

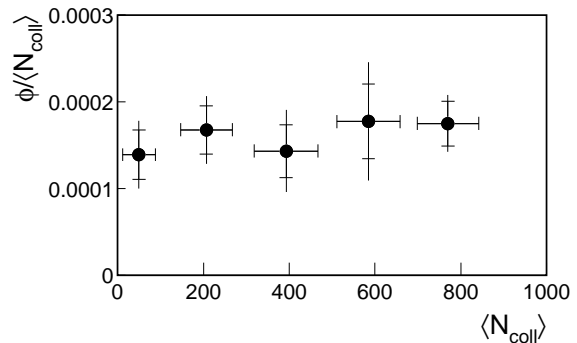


FIG. 9: The normalized fiducial yield of ϕ mesons per number of binary collisions, $\langle N_{coll} \rangle$, as a function of $\langle N_{coll} \rangle$. The accepted rapidity region is $1.2 < y < 1.6$.

~ 0.9 and ~ 0.7 , respectively [9, 25]. The narrow K^- width has been attributed to the higher threshold and more restricted phase space for K^- production. Since the thresholds for K^- and ϕ production in $p + p$ collisions are very similar, we assume that the ϕ and K^- have Gaussian rapidity distributions with approximately equal widths in central Au + Au collisions. We then estimate that our fiducial yield corresponds to about 20% of the total yield. Using the parameterization described in Appendix A for the ϕ yield in $p + p$ collisions as a function of center of mass energy, \sqrt{s} , the yield of ϕ 's per binary collision in Au + Au collisions is about 50% of the ϕ yield in $p + p$ collisions at this energy. This observation seems contrary to the usual expectation of enhanced strangeness production in Au + Au collisions. We discuss this point further in Sec. IV C.

Using E866 data on the total yields of K^+ and K^- normalized to $\langle N_{coll} \rangle$, a similar scaling proportional to $\langle N_{coll} \rangle$ is observed. It appears as if the mechanisms for the production of K^+ 's, K^- 's, and ϕ 's all have a similar dependence on the centrality of the collisions, and this dependence is consistent with a scaling with the number of binary collisions, $\langle N_{coll} \rangle$. This observation suggests that hard binary collisions might play an important role in strangeness production in heavy-ion collisions.

Our observation that ϕ and kaon production scale similarly and faster than linearly with $\langle N_{pp} \rangle$ therefore provides an essential test of the details contained within rescattering models. The rescattering model that suggests the importance of contributions from KY and $K\bar{K}$ collisions in the increase of ϕ production in central A + A collisions [24] can be ruled out; if such contributions were dominant, combinatorial considerations would lead to the expectation that ϕ production should increase faster than kaon production with centrality. This is incompatible with our observation that ϕ and kaon production show similar scaling with centrality.

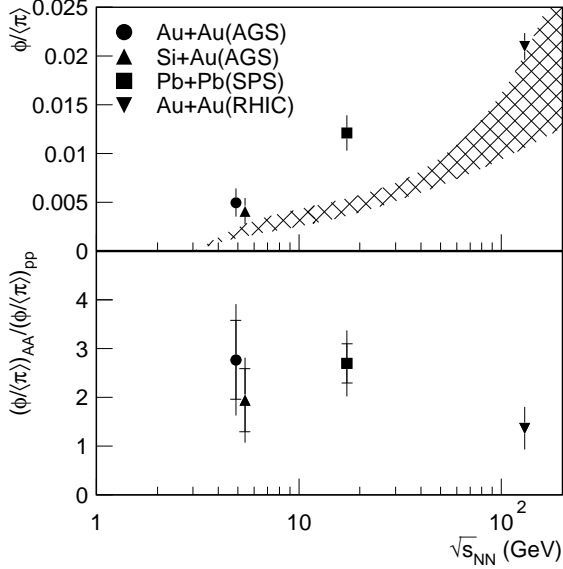


FIG. 10: Ratios of $\phi/\langle\pi\rangle$ in central heavy-ion and $p+p$ interactions as a function of $\sqrt{s_{NN}}$ (top panel) and double ratios of A + A over $p+p$ (bottom panel). For the E917 and STAR points, fiducial yield ratios are plotted; for the other two points, total yield ratios are shown instead. The hatched area represents the ratio of total yields in $p+p$ collisions, based on the parameterization discussed in Appendix A. The cross bars in the bottom panel indicate the contribution to the total errors from the uncertainty on $\phi/\langle\pi\rangle$ in central heavy-ion interactions.

C. Dependence of ϕ/π , ϕ/K^+ , and ϕ/K^- ratios on $\sqrt{s_{NN}}$ in A + A and $p+p$ reactions

In order to further explore the mechanism responsible for the approximate scaling of the ϕ yield with $\langle N_{coll} \rangle$ observed in our data, we compare our results with other measurements of ϕ production in heavy-ion collisions at different reaction energies.

The excitation functions of the ϕ/π , ϕ/K^+ , and ϕ/K^- ratios in central heavy-ion collisions are shown in Figs. 10, 11, and 12. The four points correspond to Au + Au collisions at the AGS (this measurement, $\sqrt{s_{NN}} = 4.87$ GeV) [9, 46], Si + Au collisions at the AGS ($\sqrt{s_{NN}} = 5.39$ GeV) [4, 8, 25], Pb + Pb collisions at the SPS ($\sqrt{s_{NN}} = 17.27$ GeV) [5, 53], and Au + Au collisions at RHIC ($\sqrt{s_{NN}} = 130$ GeV) [7, 14]. These plots must be interpreted with some care. Most obviously, the collisional system is different in each case; in particular, the various particle yields are not guaranteed to scale in the same way when passing from the Si + Au system to the heavier systems. In addition, the points for Au+Au collisions at the AGS and RHIC represent fiducial-yield ratios (the AGS point is for the fiducial yield over $1.2 < y < 1.6$, and the RHIC point is for the central unit of rapidity), while the other two points are ratios of yields over all

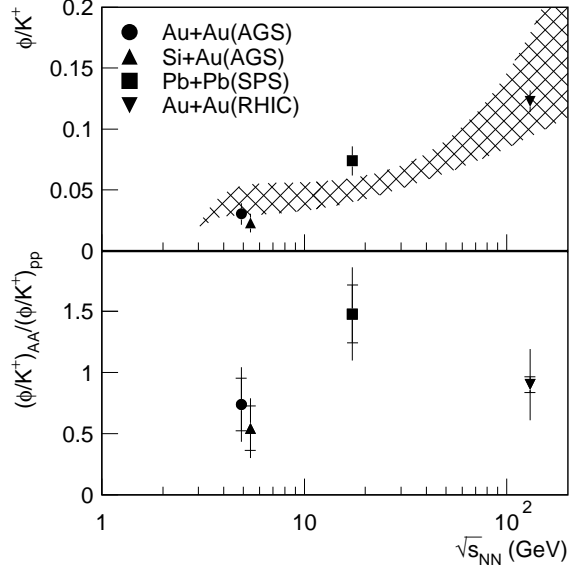


FIG. 11: Same as Fig. 10 for the ratios of ϕ/K^+ .

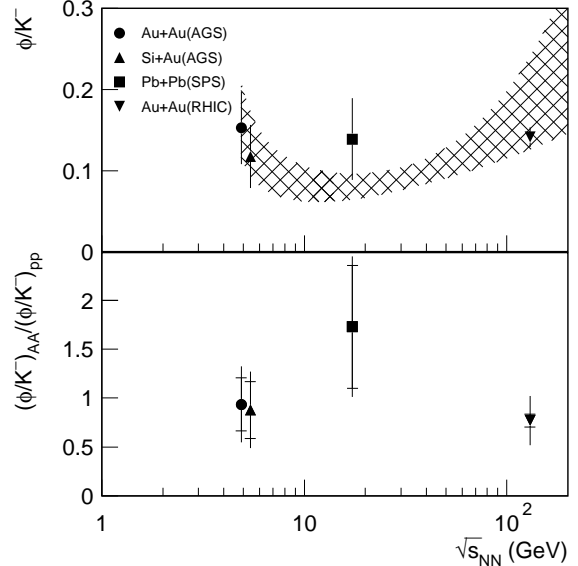


FIG. 12: Same as Fig. 10 for the ratios of ϕ/K^- .

phase space. Nor have we applied any corrections in the comparisons with $p+p$ collisions to take into account the isospin averaging of yields from $p+p$, $n+n$, and $p+n$ collisions [9, 25, 54]. Nevertheless, two observations can be made.

Our first observation is that the ϕ/π ratios for A + A collisions are notably enhanced with respect to their values for $p+p$ collisions for all points except at the highest

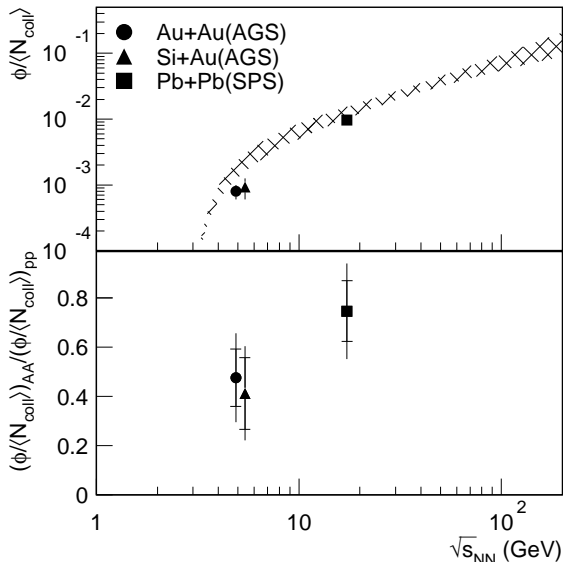


FIG. 13: Same as Fig. 10 for the ratios of $\phi/\langle N_{\text{coll}}\rangle$, where $\langle N_{\text{coll}}\rangle$ is the number of binary collisions. For the E917 data point, an estimated total ϕ yield is plotted as described in the text.

energy in Fig. 10. In $p + p$ collisions, ϕ/π increases with $\sqrt{s_{NN}}$, in large part because of the larger production threshold for ϕ mesons. In heavy-ion collisions, the ϕ/π ratios are enhanced by factors of 2–3, at least up to SPS energies, but seem to show the same energy dependence observed in $p + p$ collisions, at least up to SPS energies. Such an enhancement in the central A+A collisions could be interpreted as due to the different scaling behaviors of ϕ and π with centrality. As discussed in Sec. IV B, the yield of ϕ 's scales with $\langle N_{\text{coll}}\rangle$ while that of π 's scales with $\langle N_{pp}\rangle$. The ratio of $\langle N_{\text{coll}}\rangle$ to $\langle N_{pp}\rangle$ is around 1 in peripheral collisions, which are similar to $p + p$ collisions, and becomes larger than 1 in central collisions. At RHIC, the ϕ/π ratio for central Au + Au collisions is about the same as that from the parameterization of the $p + p$ data. It might be speculated that the primary production channels for ϕ 's and/or π 's at RHIC energies are different from those at AGS and SPS energies.

The second observation is that the ϕ/K ratios for A+A collisions are only marginally enhanced with respect to their values for $p + p$ collisions, and show relatively little variation as a function of energy as seen in Fig. 11 and Fig. 12. Our parameterization of the $p + p$ cross section for ϕ production suggests that the ϕ/K^- ratio increases as $\sqrt{s_{NN}}$ approaches the threshold value from above for the reaction $pp \rightarrow pp\phi$. The ϕ/K^- ratios in heavy-ion data seem to follow the energy dependence observed in $p + p$ collisions rather reasonably.

It is interesting to see if the data points from other systems and energies obey the scaling with $\langle N_{\text{coll}}\rangle$ as well.

The ratio $\phi/\langle N_{\text{coll}}\rangle$ for central A + A collisions at the AGS and SPS is plotted in Fig. 13. For the comparison, we are forced to assume a value for the ϕ rapidity width for our measurement. A width of $\sigma_y = 0.71$ equal to the measured K^- width is used, as explained in the previous section, and we plot our point with an additional 20% systematic uncertainty corresponding to a range of values for σ_y from 0.6 (overlap of K^+ and K^- rapidity distributions) to 0.9 (K^+ rapidity distribution). The RHIC point is not included in this comparison, because there is no reasonable way to extrapolate the fiducial yield to all of phase space. The ratio $(\phi/\langle N_{\text{coll}}\rangle)_{A+A}/(\phi/\langle N_{\text{coll}}\rangle)_{p+p}$ is consistent with ~ 0.5 – 0.7 for all three points from the AGS and SPS. Our comparison is by no means precise. However, it does seem that the yield of ϕ 's per binary collision, modulo the effects of threshold and center-of-mass energy dependence, is approximately constant across the three collisional systems studied. Furthermore, instead of there being an enhancement in the ϕ yield per binary collision in heavy-ion collisions, this double ratio is less than 1. This might reflect the effect of ϕ absorption in the nuclear fireball, as the inelastic cross section of the ϕ on nucleons (~ 8 – 10 mb) is a significant component of the total interaction cross section (~ 8 – 12 mb) [41, 55].

V. SUMMARY

In conclusion, we have studied ϕ production in Au+Au collisions at 11.7A GeV/c around midrapidity as a function of collision centrality. The yield per projectile participant shows a steady rise toward central collisions. This enhanced production in central collisions is stronger than that of non-strange π mesons as seen from the increasing ϕ/π ratio with centrality. The ratios ϕ/K^+ and ϕ/K^- are approximately constant with $\langle N_{pp}\rangle$. The yield of ϕ 's, like the yields of K^+ and K^- , is seen to scale with $\langle N_{\text{coll}}\rangle$, the number of binary collisions, and this observation is incompatible with predictions from some rescattering models of ϕ production, in which ϕ production increases faster than kaon production with centrality due to combinatorial considerations. Finally the yield of ϕ 's per binary collision in A + A collisions is about 50–70% of the ϕ yield in $p + p$ collisions at AGS and SPS energies. That the yield of ϕ 's per binary collision in A + A collisions is smaller than that in $p + p$ collisions might signal the effect of ϕ absorption by nucleons in heavy-ion collisions.

Acknowledgments

This work has been supported by the U.S. Department of Energy under contracts with ANL (No. W-31-109-ENG-38), BNL (No. DE-AC02-98CH10886), MIT (No. DE-AC02-76ER03069), UC Riverside (No. DE-FG03-86ER40271), UIC (No. DE-FG02-94ER40865), and the University of Maryland (No. DE-FG02-93ER40802); by the National Science Foundation under contract with the

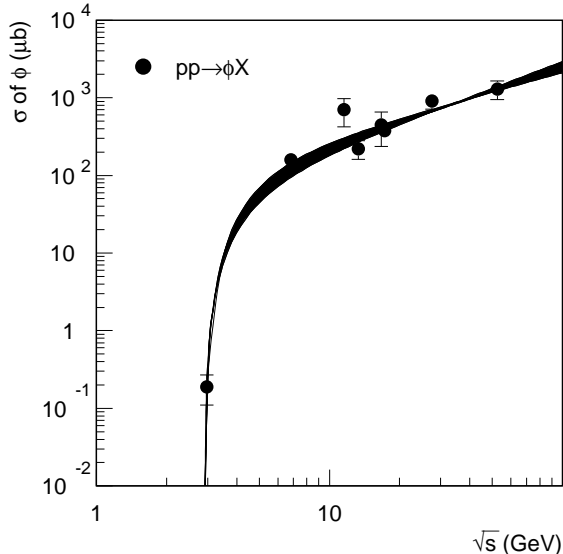


FIG. 14: Parameterization of the ϕ yield in $p+p$ interactions. The data points are from Refs. [5, 48, 56]. The fit is discussed in the text.

University of Rochester (No. PHY-9722606); and by the Ministry of Education and KOSEF (No. 951-0202-032-2) in Korea.

APPENDIX A: PARAMETERIZATION OF ϕ PRODUCTION AS A FUNCTION OF \sqrt{s} IN $p+p$ COLLISIONS

The ϕ yield in $p+p$ collisions provides a useful benchmark for the interpretation of ϕ yields in heavy-ion col-

lisions. There are various existing measurements of the inclusive total cross section for ϕ production in $p+p$ collisions for $5 < \sqrt{s} < 60$ GeV [5, 48, 56] that can be extrapolated to the values of $\sqrt{s_{NN}}$ for which heavy-ion data exist. (Note that the point at $\sqrt{s} = 2.90$ GeV from Ref. [48], while technically an exclusive measurement in the $pp \rightarrow ppK^+K^-$ channel, is also an inclusive measurement, since no other channels with a ϕ or K^- in the final state are kinematically allowed at this energy.) We have fit these measurements with a form used to parameterize results on vector-meson production cross sections in $p+p$ collisions obtained from one-pion exchange calculations [57] and the Lund String Model [58]:

$$\begin{aligned} \sigma(pp \rightarrow \phi X) &= a(1-x)^b x^c \\ x &\equiv s_{\text{thresh}}/s \\ s_{\text{thresh}} &= 8.38 \text{ GeV}^2 \end{aligned} \quad (\text{A1})$$

The results of our fit are shown in Fig. 14. We obtain $a = 74^{+36}_{-24} \mu\text{b}$, $b = 2.05^{+0.22}_{-0.18}$, and $c = 1.56^{+0.30}_{-0.27}$. For comparison with heavy-ion data, we obtain yields by dividing the ϕ cross sections for each value of $\sqrt{s_{NN}}$ by the inelastic $p+p$ cross section. For Au + Au collisions at the AGS, $\sqrt{s_{NN}} = 4.87$ GeV, and our parameterization of the $p+p$ data gives a yield of 0.00169 ± 0.00042 at this energy.

For K and π production in $p+p$ reactions, we use the multiplicity parameterizations in Ref. [59]. The smallest \sqrt{s} for the ranges of parameterization for π , K^+ and K^- are 3.0, 2.98, and 5.03 GeV, respectively.

-
- [1] S. Okubo, Phys. Lett. B **5**, 165 (1963); G. Zweig, CERN report NO. 8419/TH, 412 (1964); I. Iizuka, Prog. Theor. Phys. Suppl. **37/38**, 21 (1966).
- [2] P. Koch, B. Müller, and J. Rafelski, Z. Phys. A **324**, 453 (1986).
- [3] A. Shor, Phys. Rev. Lett. **54**, 1122 (1985).
- [4] Y. Akiba *et al.*, Phys. Rev. Lett. **76**, 2021 (1996).
- [5] S.V. Afanasiev *et al.*, Phys. Lett. B **491**, 59 (2000).
- [6] B. Alessandro *et al.*, Phys. Lett. B **555**, 147 (2003).
- [7] C. Adler *et al.*, Phys. Rev. C **65**, 041901(R) (2002).
- [8] T. Abbott *et al.*, Phys. Rev. Lett. **64**, 847 (1990).
- [9] L. Ahle *et al.*, Phys. Rev. C **58**, 3523 (1998).
- [10] L. Ahle *et al.*, Phys. Lett. B **476**, 1 (2000).
- [11] T.A. Armstrong *et al.*, Phys. Rev. C **59**, 2699 (1999).
- [12] B.B. Back *et al.*, Phys. Rev. Lett. **87**, 242301 (2001).
- [13] E. Anderson *et al.*, Phys. Lett. B **433**, 209 (1998); E. Anderson *et al.*, Phys. Lett. B **449**, 401 (1999).
- [14] K. Adcox *et al.*, Phys. Rev. Lett. **88**, 242301 (2002).
- [15] R. Mattiello *et al.*, Phys. Rev. Lett. **63**, 1459 (1989).
- [16] Y. Pang, T.J. Schlagel, and S.H. Kahana, Phys. Rev. Lett. **68**, 2743 (1992).
- [17] B.A. Li and C.M. Ko, Phys. Rev. C **52**, 2037 (1995).
- [18] P. Braun-Munzinger *et al.*, Phys. Lett. B **344**, 43 (1995); J. Cleymans *et al.*, Z. Phys. C **74**, 319 (1997).
- [19] I. Chemakin *et al.*, Phys. Rev. Lett. **85**, 4868 (2000).
- [20] M.B. Green *et al.*, Nuovo Cimento A **29**, 123 (1975); A. Donnachie and P.V. Landshoff, Nucl. Phys. B **112**, 233 (1976).
- [21] J. Ellis *et al.*, Phys. Lett. B **353**, 319 (1995).
- [22] W.S. Chung *et al.*, Phys. Lett. B **401**, 1 (1997).
- [23] M. Berenguer, H. Sorge, and W. Greiner, Phys. Lett. B **332**, 15 (1994).
- [24] C.M. Ko and B.H. Sa, Phys. Lett. B **258**, 6 (1991).
- [25] L. Ahle *et al.*, Phys. Rev. C **60**, 044904 (1999).
- [26] F.Q. Wang, J. Phys. G **27**, 283 (2001).
- [27] J.C. Dunlop and C.A. Ogilvie, Phys. Rev. C **61**, 031901

- (2000).
- [28] L. Ahle *et al.*, Phys. Lett. B **490**, 53 (2000).
- [29] B.B. Back *et al.*, Phys. Rev. Lett. **86**, 1970 (2001).
- [30] B.B. Back *et al.*, Phys. Rev. C **66**, 054901 (2002).
- [31] T. Abbott *et al.*, Nucl. Instrum. Meth. A **290**, 41 (1990).
- [32] H. Xiang, Ph.D. Thesis, Univ. of California, Riverside, 1999; J.C. Dunlop, Ph.D. Thesis, MIT, 1999; G. Heintzelman, Ph.D. Thesis, MIT, 1999; M.D. Moulson, Ph.D. Thesis, Columbia Univ., 2001.
- [33] W.A. Zajc, AIP Conf. Proc. **243**, 415 (1992).
- [34] L.Y. Geer *et al.*, Phys. Rev. C **52**, 334 (1995).
- [35] R.J. Glauber and G. Matthiae, Nucl. Phys. B **21**, 135 (1970).
- [36] T. Abbott *et al.*, Phys. Rev. C **44**, 1611 (1991).
- [37] G.I. Kopylov, Phys. Lett. B **50**, 472 (1974).
- [38] J.D. Jackson, Nuovo Cimento **34**, 6692 (1964).
- [39] S. Baker and R.D. Cousins, Nucl. Instrum. Meth. **221**, 437 (1984).
- [40] E. Schnedermann, J. Sollfrank, and U. Heinz, Phys. Rev. C **48**, 2462 (1993).
- [41] G. McClellan *et al.*, Phys. Rev. Lett. **26**, 1593 (1971); H.-J. Behrend *et al.*, Phys. Lett. B **56**, 408 (1975); T.H. Bauer *et al.*, Rev. Mod. Phys. **50**, 261 (1978); H. Joos, Phys. Lett. B **24**, 103 (1967).
- [42] H. van Hecke, H. Sorge, and N. Xu, Phys. Rev. Lett. **81**, 5764 (1998).
- [43] E.V. Shuryak, Nucl. Phys. A **661**, 119c (1999).
- [44] S.C. Johnson, B.V. Jacak, and A. Drees, Eur. Phys. J. C **18**, 645 (2001).
- [45] P. Filip and E.E. Kolomeitsev, Phys. Rev. C **64**, 054905 (2001).
- [46] L. Ahle *et al.*, Phys. Rev. C **59**, 2173 (1999).
- [47] L. Ahle *et al.*, Phys. Rev. C **60**, 064901 (1999).
- [48] F. Balestra *et al.*, Phys. Rev. C **63**, 024004 (2001).
- [49] J. Ellis *et al.*, Nucl. Phys. A **673**, 256 (2000).
- [50] V.V. Anisovich *et al.*, Nucl. Phys. B **133**, 477 (1978).
- [51] K. Kadija *et al.*, Z. Phys. C **66**, 393 (1995).
- [52] L. Ahle *et al.*, Phys. Rev. C **57**, R466 (1998).
- [53] S.V. Afanasiev *et al.*, Phys. Rev. C **66**, 054902 (2002).
- [54] M. Gazdzicki and O. Hansen, Nucl. Phys. A **528**, 754 (1991).
- [55] R. Bailey *et al.*, Z. Phys. C **22**, 125 (1984).
- [56] F. Balestra *et al.*, Phys. Lett. B **468**, 7 (1999); V. Blobel *et al.*, Phys. Lett. B **59**, 88 (1975); M. Antipov *et al.*, Phys. Lett. B **110**, 326 (1982); C. Daum *et al.*, Nucl. Phys. B **186**, 205 (1981); D. Drijard *et al.*, Z. Phys. C **9**, 293 (1981).
- [57] A.A. Sibirtsev, Nucl. Phys. A **604**, 455 (1996).
- [58] W. Cassing and E.L. Bratkovskaya, Phys. Rept. **308**, 65 (1999).
- [59] A.M. Rossi *et al.*, Nucl. Phys. B **84**, 269 (1975).